INAF

ISTITUTO NAZIONALE DI ASTROFISICA
OSSERVATORIO ASTROFISICO DI ARCETRI

UNIVERSITÀ DEGLI STUDI FIRENZE

Lecture IX: Kinematics and dynamics of early-type galaxies.

Astrophysics of Galaxies 2019-2020

Stefano Zibetti - INAF Osservatorio Astrofisico di Arcetri

Lecture IX

Kinematic from absorption lines spectra

- Comparison of observed spectrum with "shifted" (→ v) and broadened (→σ) spectrum of a star

- Today a composite spectrum of a mixture of stars is used: kinematics and weights of different stellar templates are fitted simultaneously

Faber & Jackson (1976)

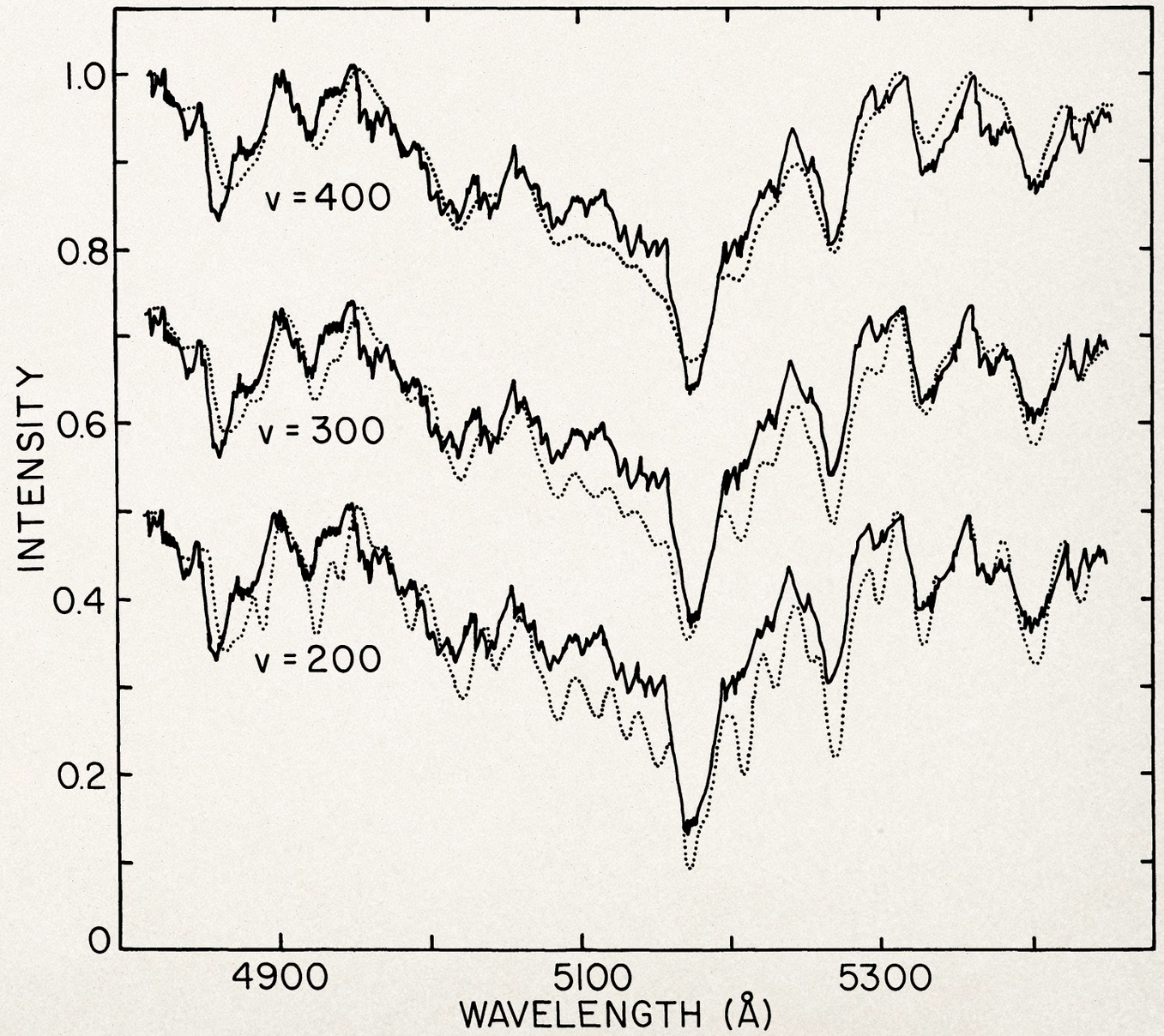

FIG. 3.—NGC 4472 compared with standard star HR 1805 (K3 III), broadened by various line-of-sight velocities (*dotted line*)

More detailed modeling...

$$\mathcal{L}(v) = \frac{e^{-(1/2)y^2}}{\sigma\sqrt{2\pi}}\left[1 + \sum_{m=3}^{M} h_m H_m(y)\right]$$

$$y = (v - V)/\sigma$$

- Gaussian "modulated" with Hermite polynomials
- m>2 require *high* SNR; usually expansions stops at m=4 (h3 and h4 terms)
- → pPXF fitting code (Cappellari & Emsellem 2004)

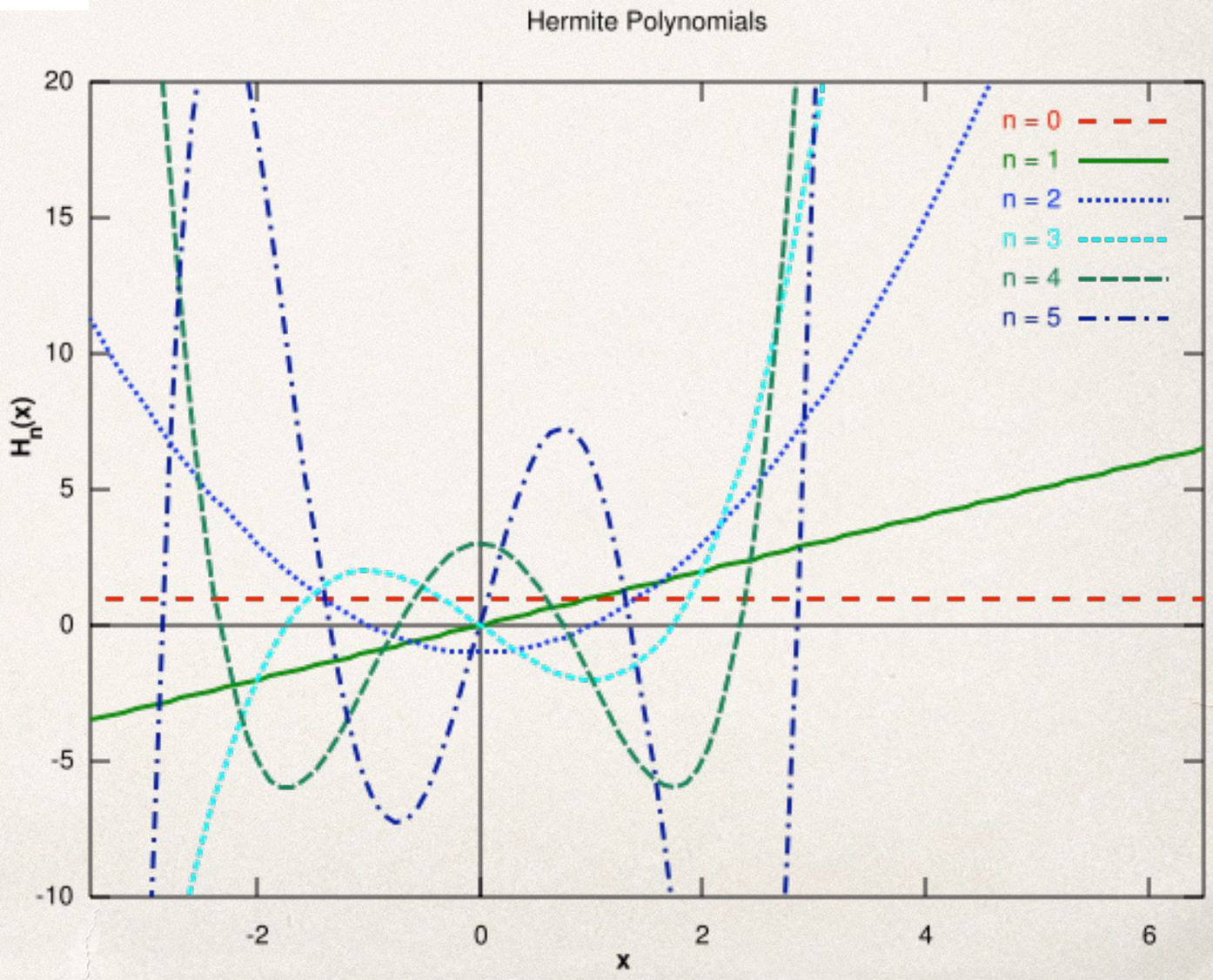

Velocity and dispersion fields of E's

- σ dominates over V: "pressure" supported rather than rotation supported systems
- ordered rotation may be present or not

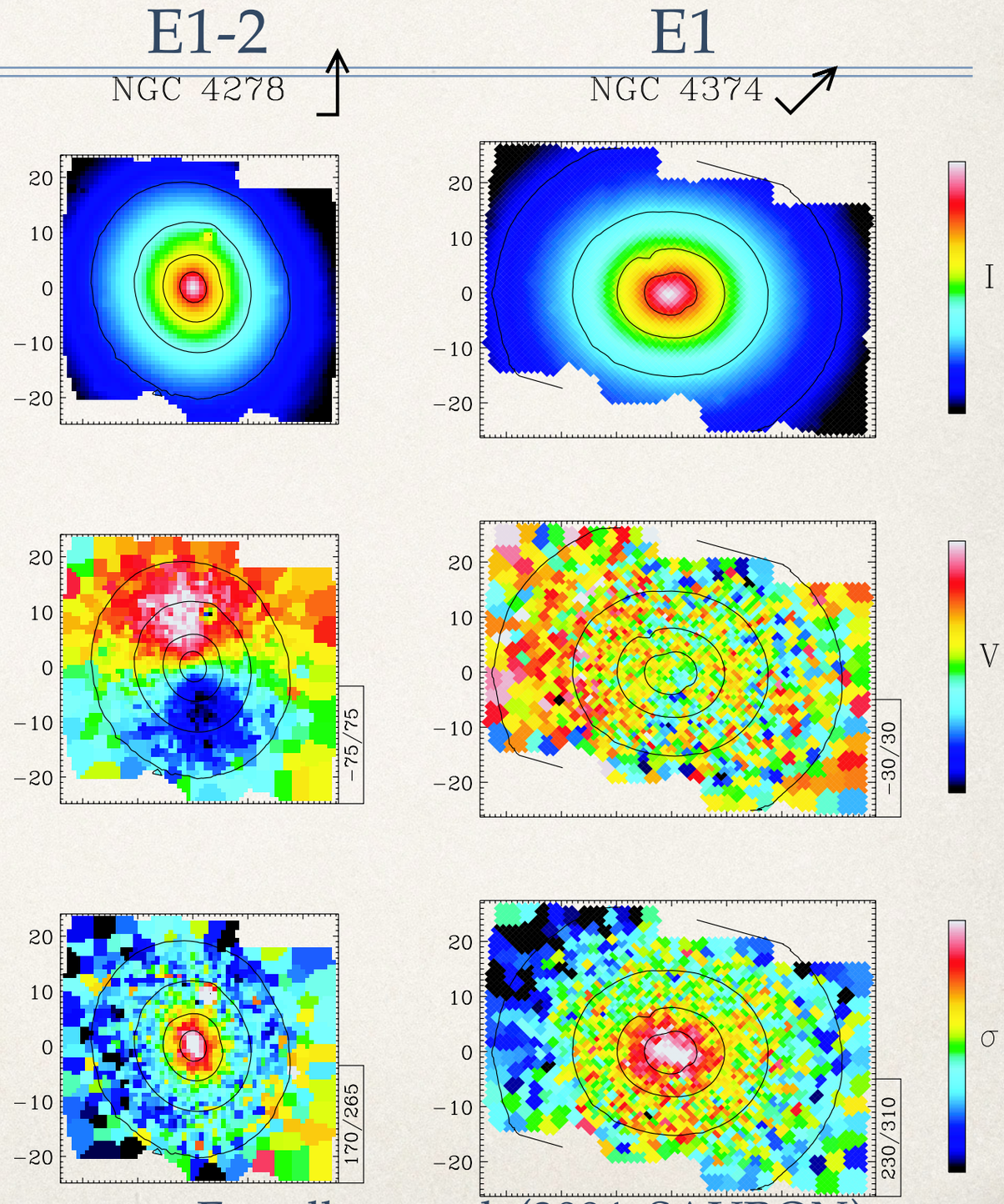

Emsellem et al. (2004, SAURON)

Central (?) velocity dispersion

- in the good old times people had one spectrum per galaxy (and still now for the largest surveys and most of the intermediate/high z galaxies) and have to live with that...

- σ_0 is not an observable to take "as is"
  - need to correct for aperture

- σ_0 is not representative of the full galaxy

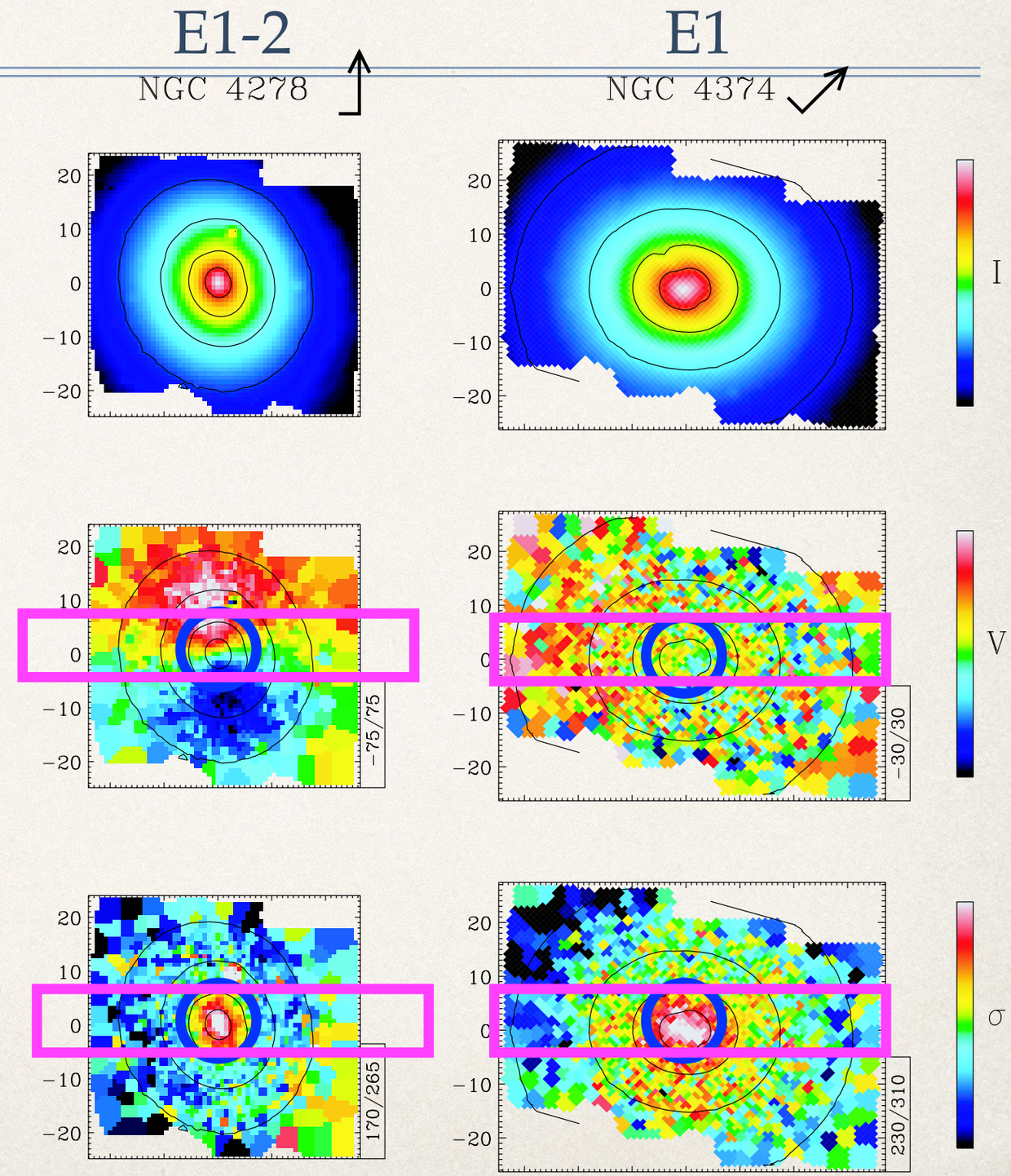

The Faber-Jackson relation

$$\sigma^2 \approx \frac{GM}{R}$$

$$\left.\begin{aligned} L = M\left(\frac{M}{L}\right)^{-1} \\ L \approx\propto R^2 \end{aligned}\right\} L \propto \sigma^4$$

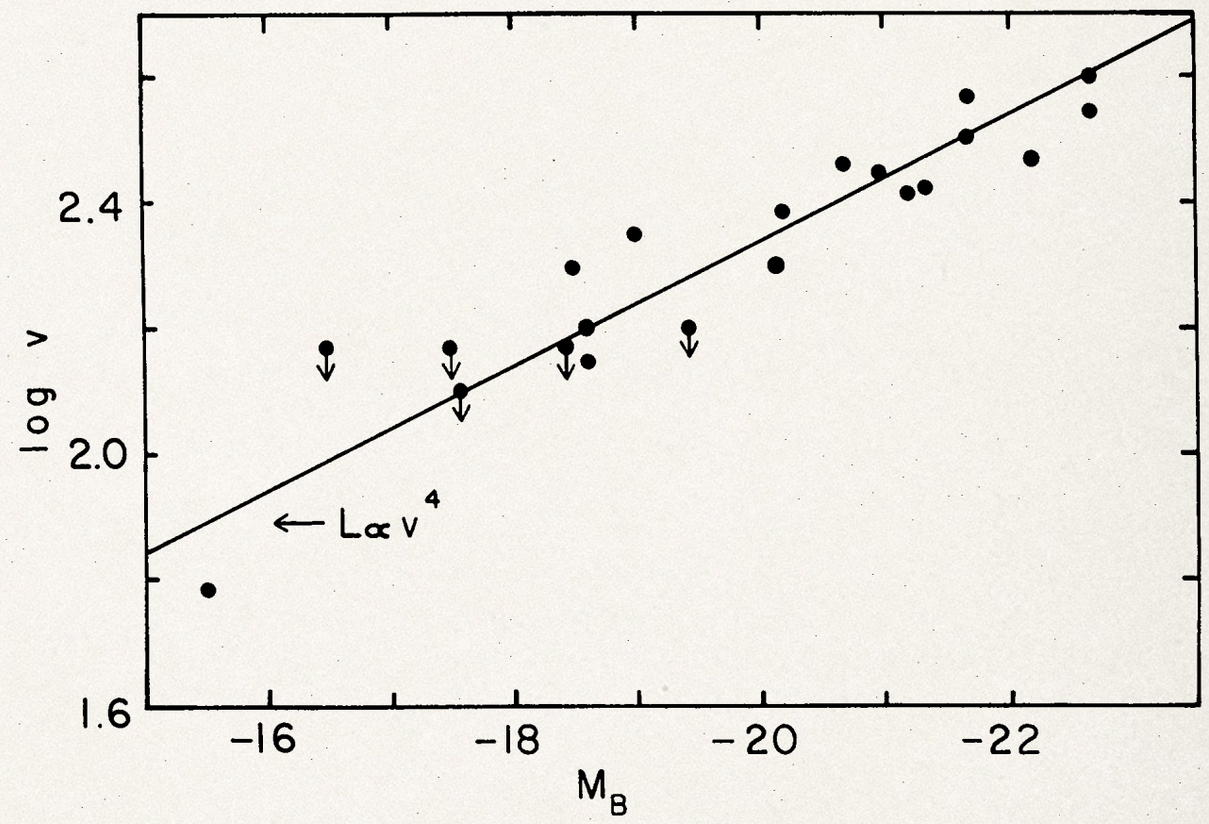

FIG. 16.—Line-of-sight velocity dispersions versus absolute magnitude from Table 1. The point with smallest velocity corresponds to M32, for which the velocity dispersion (60 km s^{-1}) was taken from Richstone and Sargent (1972).

Faber & Jackson (1976)

The F-J relation reloaded: SDSS

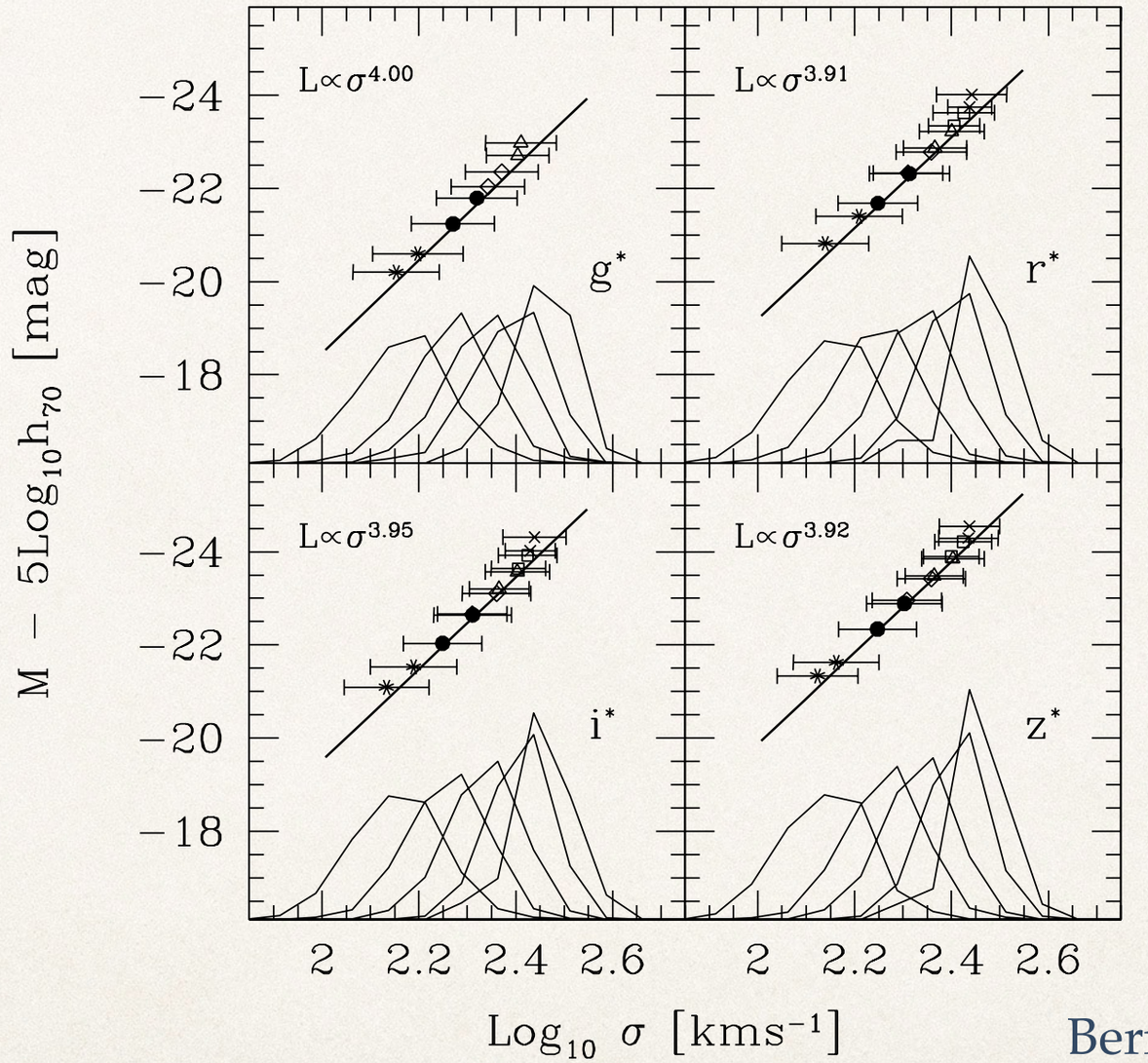

~9000 ETGs

Bernardi et al. (2003, paper II)

FIG. 4.—Relation between luminosity L and velocity dispersion σ. Stars, circles, diamonds, triangles, squares, and crosses show the error-weighted mean value of log σ for a small range in luminosity in each volume-limited catalog (see text for details). (Only catalogs containing more than 100 galaxies are shown.) Error bars show the rms scatter around this mean value. Solid line shows the maximum likelihood estimate of this relation, and the label in the top left shows the scaling it implies. Histograms show the distribution of log σ in small bins in luminosity. They were obtained by stacking together nonoverlapping volume-limited catalogs to construct a composite catalog, and then dividing the composite catalog into five equal-sized bins in luminosity.

The fundamental plane

- Djorgovski & Davis (1987)
- Dressler et al. (1987)
- Faber et al. (1987)
- Link between size, dynamics and surface brightness
- Since size is the only distance-dependent quantity, the FP relation is an excellent distance indicator

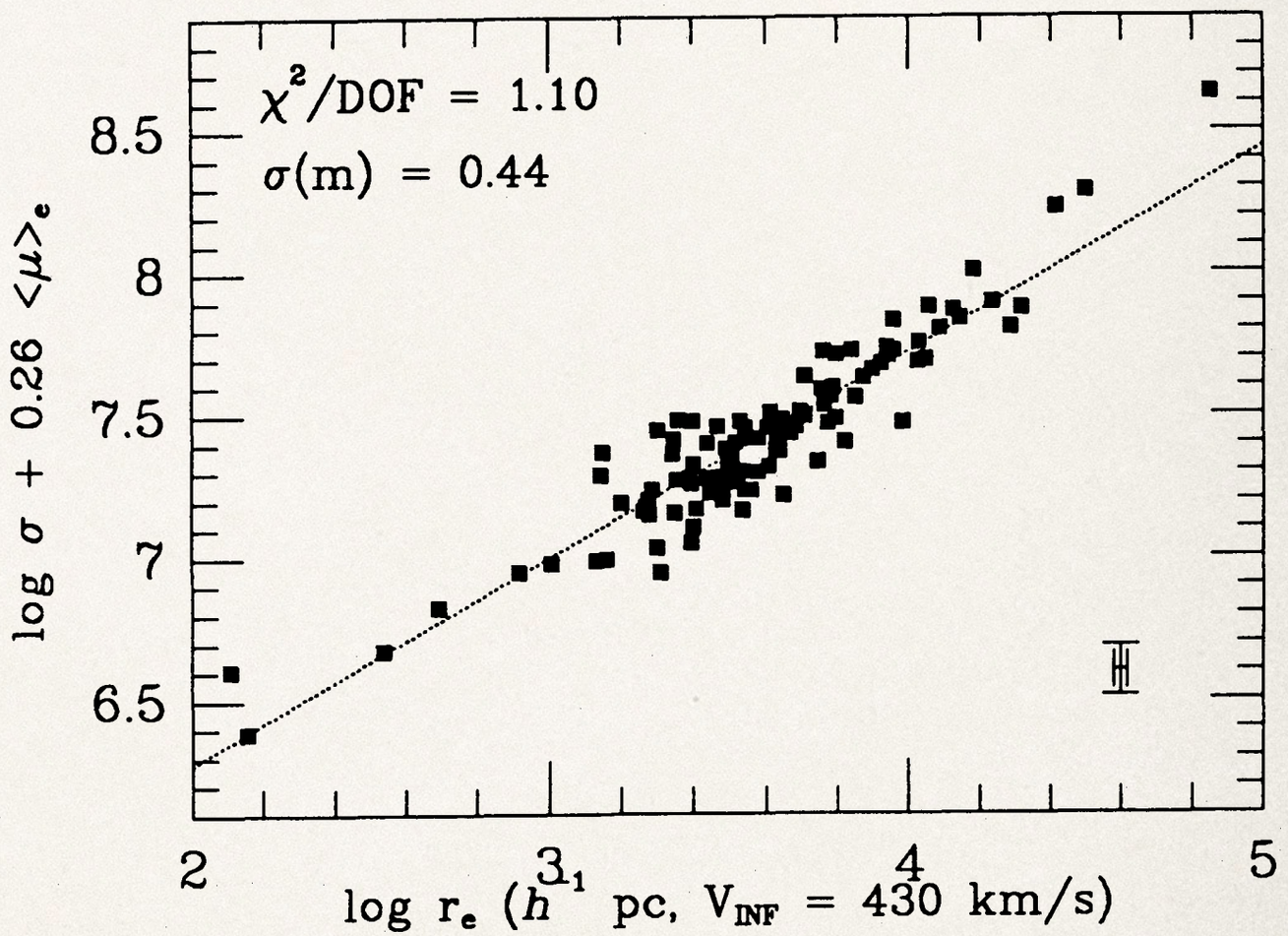

Djorgovski & Davis (1987)

FP reloaded: SDSS

Bernardi et al. (2003, paper III)

- Important to define the quantities properly!
- r is chosen as the effective radius (half light)
- σ is corrected to represent the dispersion within r/8, assuming a "standard" dispersion curve (eg Jørgensen+95)

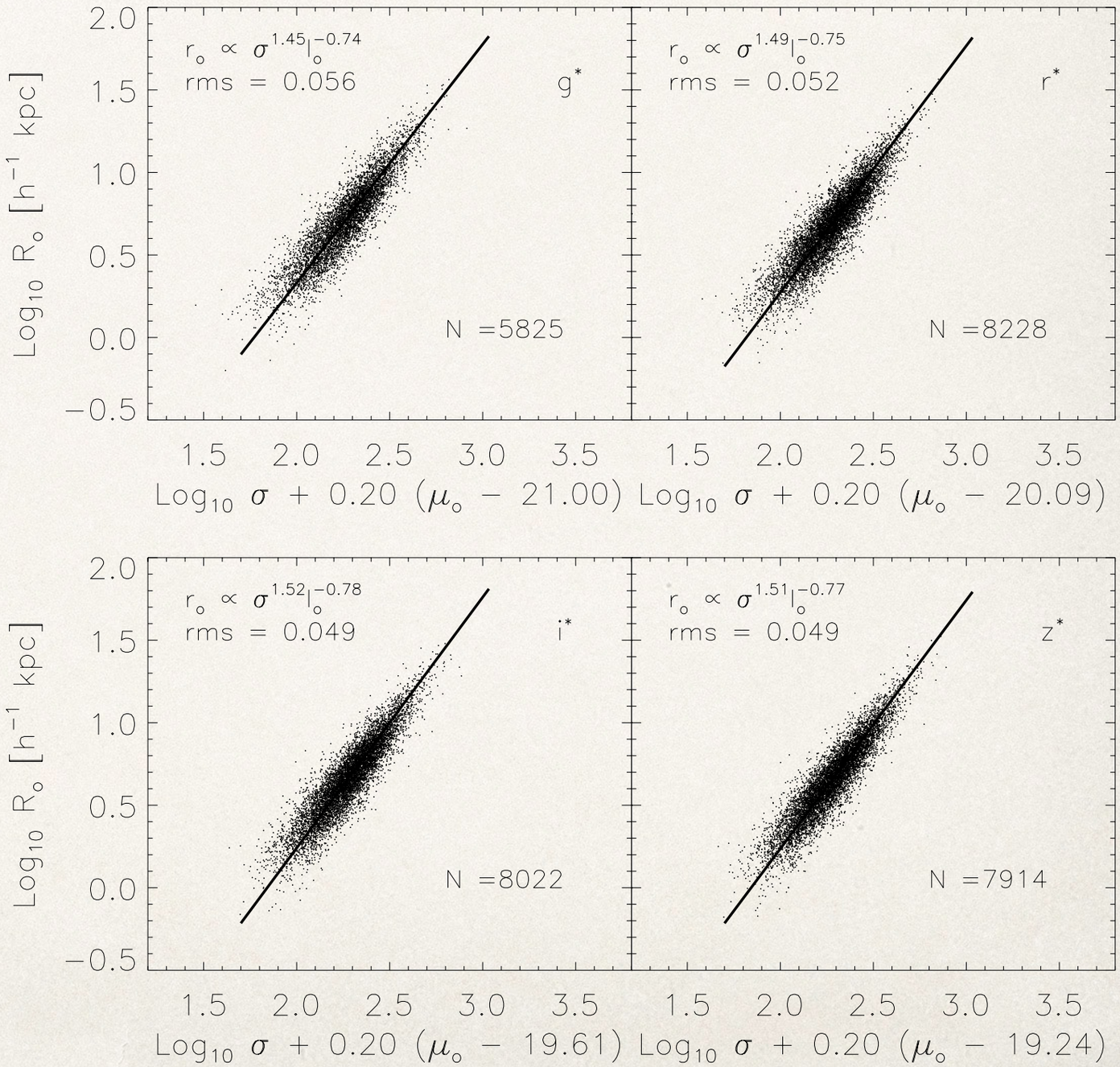

Virial interpretation and the tilt of the FP

$$\sigma^2_{\rm vir} \propto \frac{GM_{\rm vir}}{2R_{\rm vir}} \propto \left(\frac{M_{\rm vir}}{L}\right) R_{\rm vir} \left(\frac{L/2}{R^2_{\rm vir}}\right)$$

$$\sigma_0^2 \propto \frac{M}{L} r_e I_e$$

$$r_e \propto \sigma_0^2 I_e^{-1} \left(\frac{M}{L}\right)^{-1} \leftrightarrow r_e \propto \sigma_0^{1.5} I_e^{-0.75} \left(\frac{M}{L}\right)^{-1}$$

- Why are the exponent different from the virial theorem?
- Systematic variations in M/L or is the transformation from virial to observed quantities not correct?

FP interpretation and the κ3 formalism

$$\sigma^2_{\rm vir} \propto \frac{GM_{\rm vir}}{2R_{\rm vir}} \propto \left(\frac{M_{\rm vir}}{L}\right) R_{\rm vir} \left(\frac{L/2}{R^2_{\rm vir}}\right)$$

- Assume proportionality between observed quantities and virial quantities

$$L = c_1 I_e r_e^2 \qquad r_e = (c_2 c_1^{-1})(M/L)^{-1} \sigma_0^2 I_e^{-1}$$

$$M = c_2 \sigma_0^2 r_e$$

- c1, c2 "structure constants"

$$\kappa_1 \propto \log (M/c_2)$$

- Introduce the new variables:

$$\kappa_2 \propto \log (c_1/c_2) \quad (M/L) I_e^3$$

$$\kappa_3 \propto \log (c_1/c_2) \quad (M/L)$$

$$\kappa_1 \equiv (\log \sigma_0^2 + \log r_e)/\sqrt{2}\,,$$

$$\kappa_2 \equiv (\log \sigma_0^2 + 2 \log I_e - \log r_e)/\sqrt{6}\,,$$

$$\kappa_3 \equiv (\log \sigma_0^2 - \log I_e - \log r_e)/\sqrt{3}\,.$$

Bender, Burstein & Faber (1992)

The $\kappa 3$ space

- κ_3-κ_1: ~edge-on projection of the FP
- κ_2-κ_1: ~face-on projection of the FP
- M/L increasing with mass (for luminous ellipticals)
- All holds **if** the "structure constants" are *constant*!

Bender, Burstein & Faber (1992)

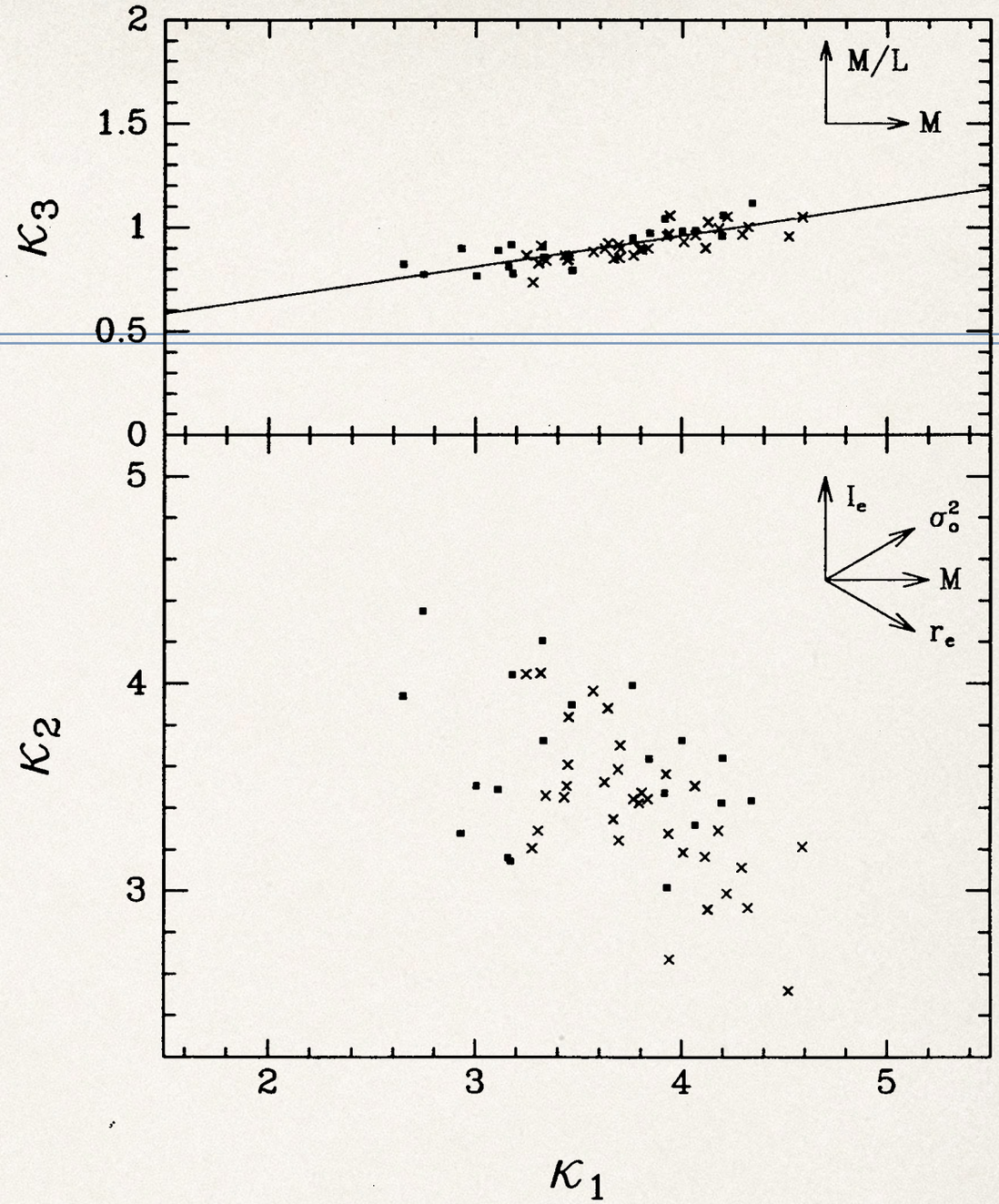

FIG. 1.—The distribution of elliptical galaxies in the Virgo Cluster and the Coma Cluster in the 3-space of the basic global parameters: central velocity dispersion (σ_o^2), surface brightness [$\log I_e = -0.4(SB_e - 27)$], and effective radius r_e. The coordinate system (κ_1, κ_2, κ_3) has been chosen to emphasize the fundamental plane while retaining physically meaningful variables: $\kappa_1 \propto \log M$, $\kappa_2 \propto \log (M/L) I_e^3$ and $\kappa_3 \propto \log M/L$. (*a*) *Upper panel:* the edge-on view of the plane occupied by Virgo (*closed boxes*) and Coma (*crosses*) ellipticals. The fundamental plane defined by the Virgo galaxies ($\kappa_3 = 0.15\ \kappa_1 + 0.36$) is shown by the straight line. (*b*) *Lower panel:* nearly face-on view of the plane.

Are the constants constant? The non-homology problem

- Elliptical galaxies present systematic variations with mass/luminosity in
  - density profiles
  - hence dispersion profiles
- Structure constants cannot be constant in a strict sense!

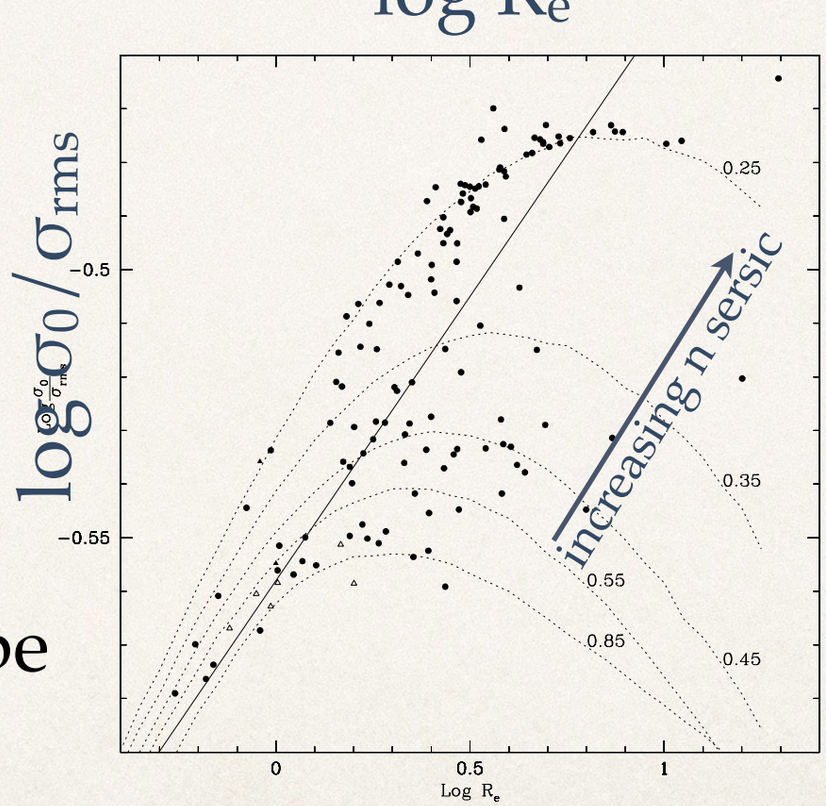

FIG. 6.—The σ_0/σ_{rms} ratio as a function of R_e. Symbols as in Fig. 4. *Solid line*: OLSB fit. *Dashed lines*: Theoretically expected relation for families of homologous galaxies modeled by Sérsic laws. Each curve is labeled with the corresponding ν index.

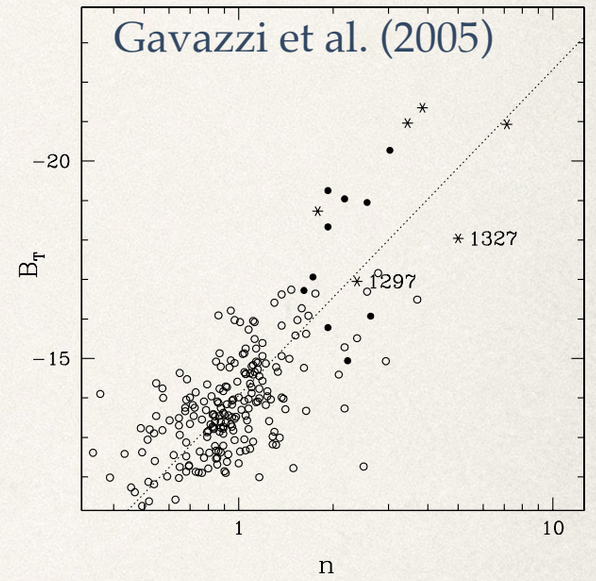

Fig. 9. The dependence of n from B_T. The dashed line gives the bisector linear regression.

Zibetti et al. (2002), based on simplified isotropic, spherically symmetric models

Dynamical modeling (following Schwarzschild 1989)

- Assume a mass distribution
  - by deprojecting the observed luminosity/mass image
    - possibly adding a DM halo
- Compute the potential
- Calculate the possible orbits and their density in 3D → different families of orbits
- Find the superposition of orbits that fit the luminosity/mass distribution and (if available) the kinematics

Orbit families: 2D potential

$$\Phi_{\rm L}(x,y) = \tfrac{1}{2}v_0^2 \ln\left(R_{\rm c}^2 + x^2 + \frac{y^2}{q^2}\right) \quad (0 < q \leq 1)$$

- log potential mimics a dark matter halo, with flat rotation curve
- Angular momentum is NOT conserved!
- Inside R_c approximate a 2D harmonic oscillator: box orbits
- possible outside R_c:
  - Loop orbits:
    - never approach the center
    - keep same rotation direction
  - Box orbits:
    - can go close to the center
    - almost radial at large R

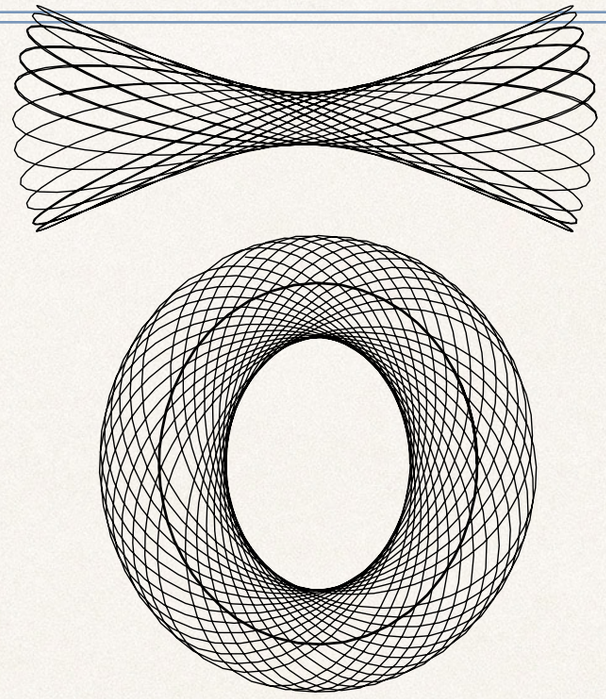

Figure 3.8 Two orbits of a common energy in the potential $\Phi_{\rm L}$ of equation (3.103) when $v_0 = 1$, $q = 0.9$ and $R_{\rm c} = 0.14$: top, a box orbit; bottom, a loop orbit. The closed parent of the loop orbit is also shown. The energy, $E = -0.337$, is that of the isopotential surface that cuts the long axis at $x = 5R_{\rm c}$.

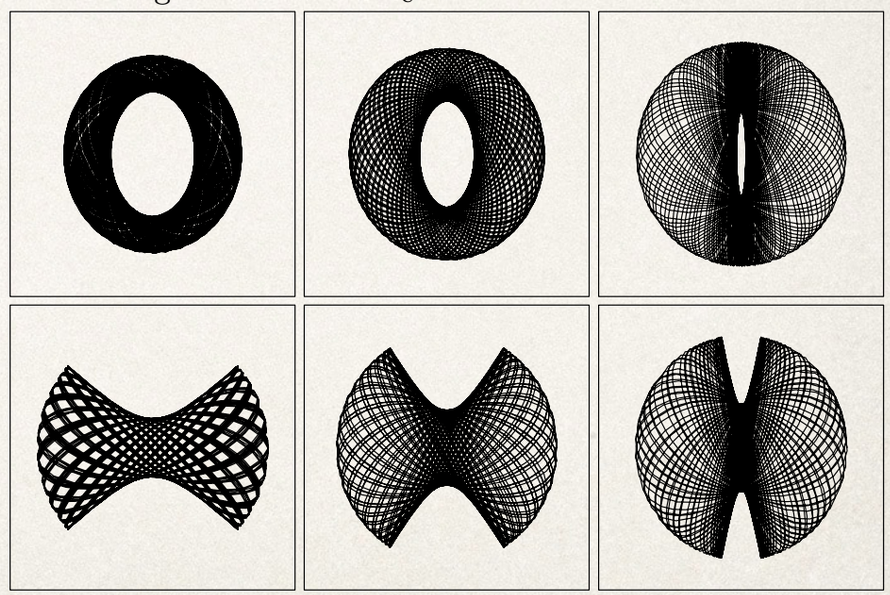

Figure 3.10 A selection of loop (top row) and box (bottom row) orbits in the potential $\Phi_{\rm L}(q = 0.9, R_{\rm c} = 0.14)$ at the energy of Figures 3.8 and 3.9.

Orbit families: triaxial potential

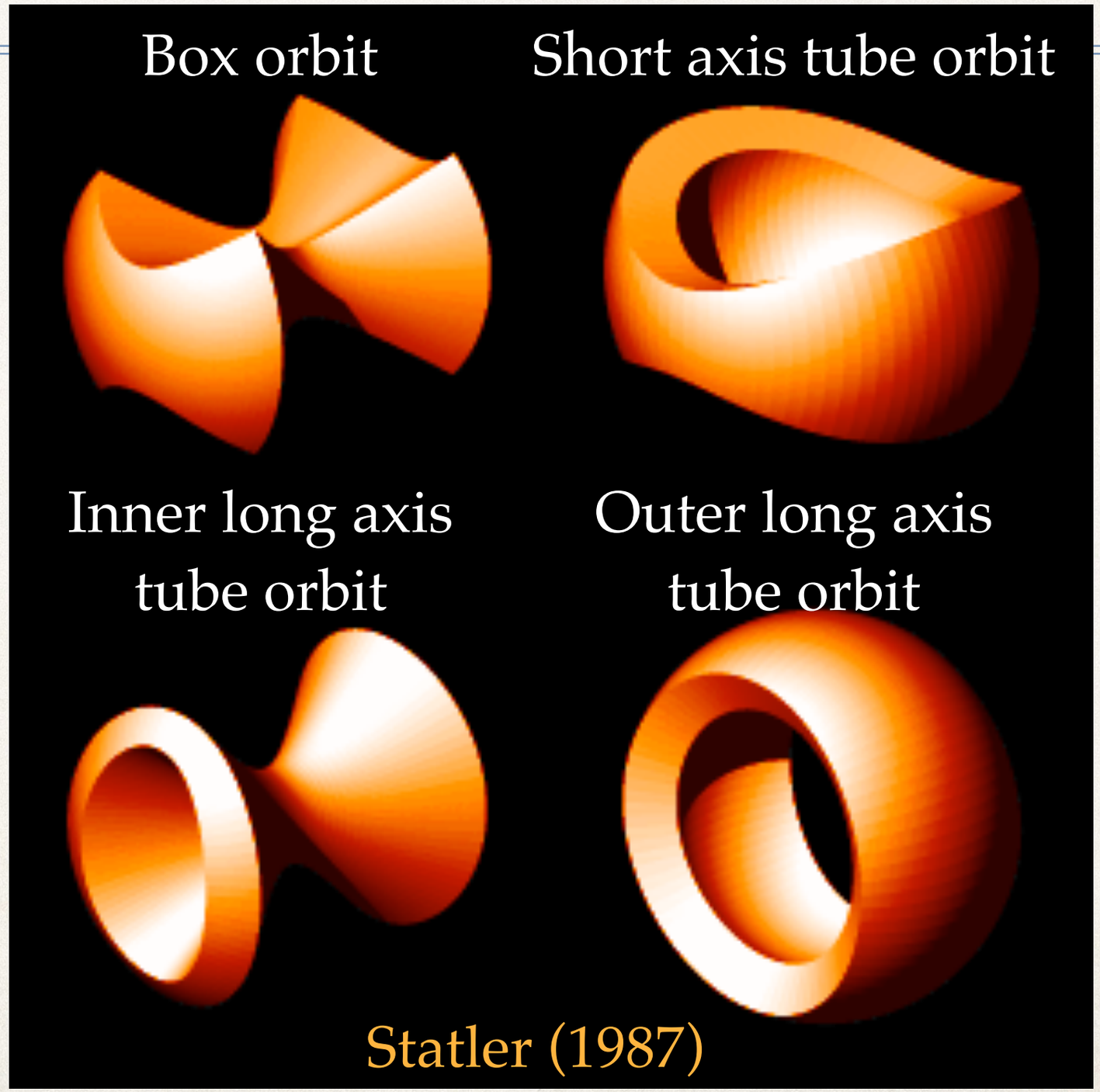

Homology holds (or as-if...)

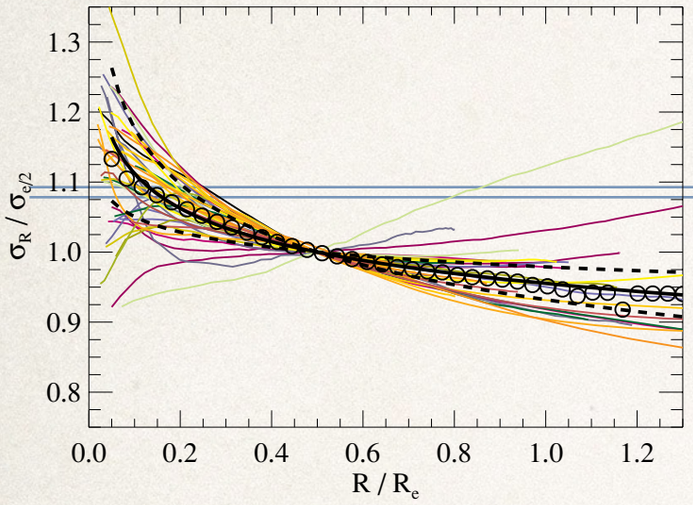

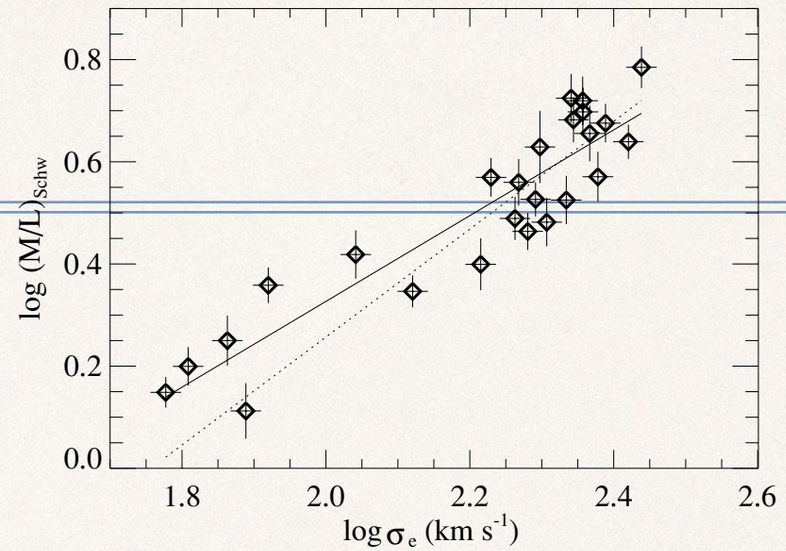

Figure 2. Luminosity-weighted second moment of the LOSVD within an aperture of radius R, normalized to its value at $R_e/2$ (see text for details).

- dispersion profiles are not homologous
- From 2- and 3-integral methods:
  - dynamical M/L increases with σ
  - M/L can be recovered from the simple virial formula and the FP

Cappellari et al. (2006, SAURON)

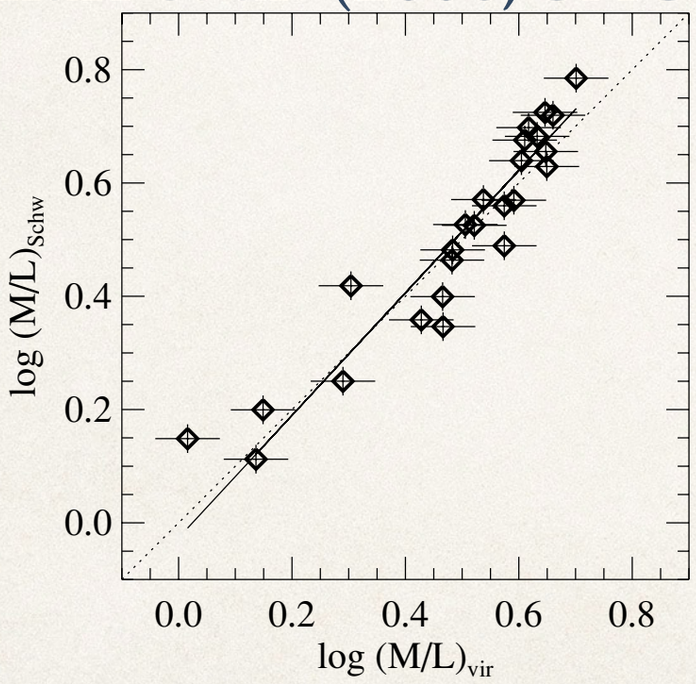

$$(M/L)_{\rm vir} = \frac{\beta\ R_{\rm e}\sigma_{\rm e}^2}{(L\,G)}$$

$$\beta = 5.0 \pm 0.1$$

Figure 13. Comparison between the $(M/L)_{\rm vir} = \beta R_{\rm e}\sigma_{\rm e}^2/(L\,G)$ derived from the virial assumption and the M/L obtained from the Schwarzschild models. The values of $(M/L)_{\rm vir}$ were scaled to match the dynamical M/L, and the best-fitting factor is $\beta = 5.0 \pm 0.1$. The solid line is a fit between the two quantities, while the dotted line represents a one-to-one correlation.

- However β is not the one expected from sersic models... things are much more complicated!

Possible origins of the FP's tilt

- Systematic variations in the rate of stellar to DM mass

- Systematic variations of the IMF

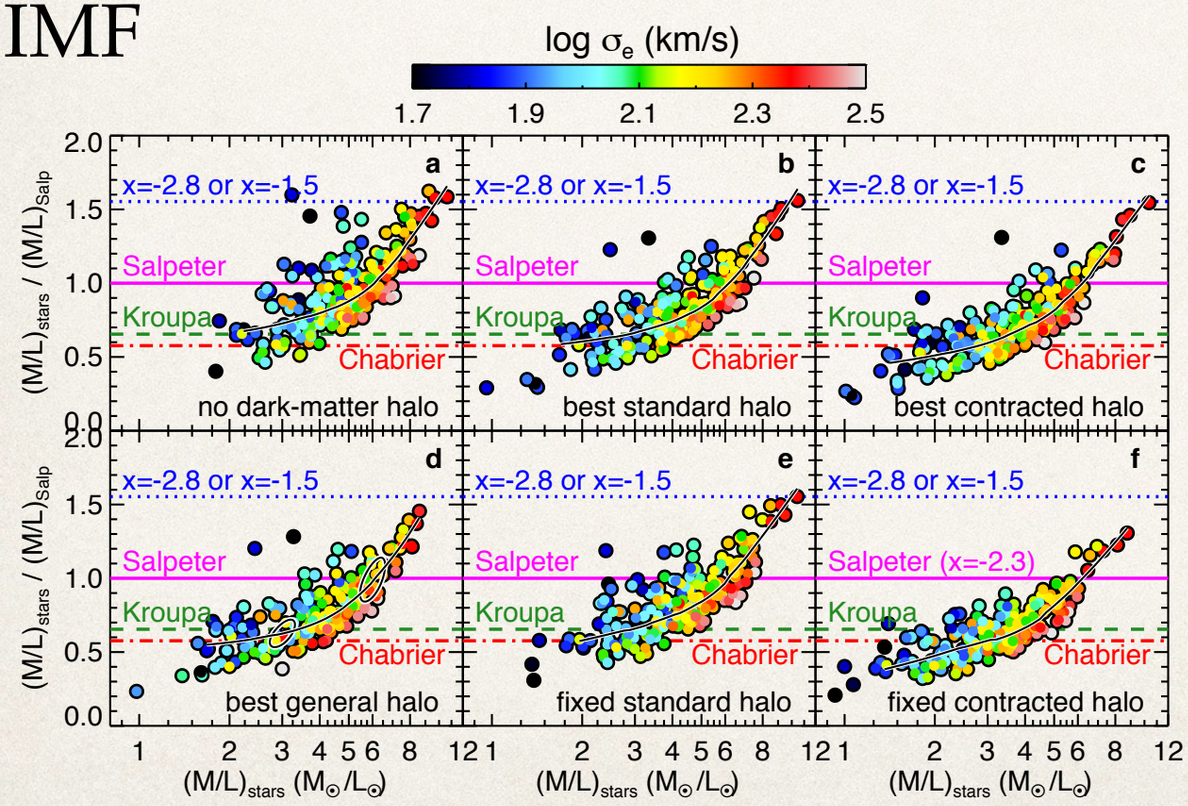

Cappellari et al. (2012)

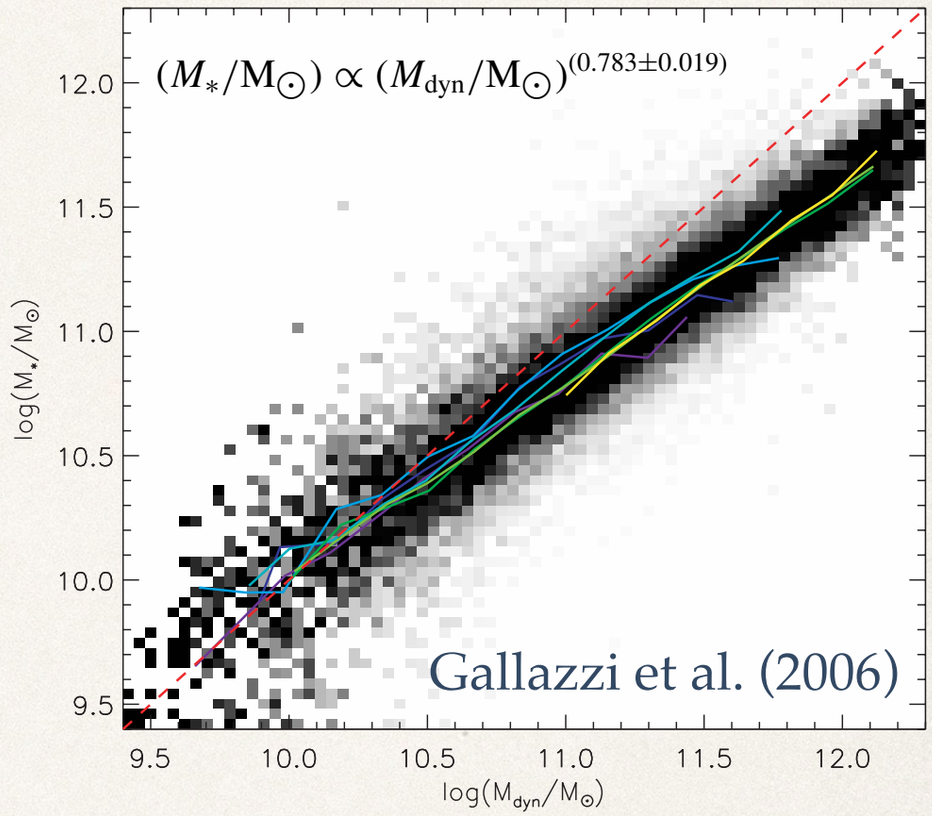

Figure 16. Relation between stellar mass and dynamical mass $M_{\rm dyn}$ estimated within the r-band Petrosian half-light radius (see equation 2). Lines of different colours represent the median relations in different bins of light-weighted age, increasing from $\log(t_r/{\rm yr}) = 9.5$ (purple) to 10.1 (yellow). The ratio between stellar and dynamical mass decreases with mass, as highlighted by the comparison with the one-to-one relation (dashed line).

The fast-slow rotators dichotomy

- In the traditional classification of early-type galaxies, fast rotators are basically S0s, while slow rotators are true ellipticals

---

- most of early-type galaxies have a significant fraction of stars in discs
- Sérsic indices of bulges of early-type galaxies are often small (n_b<3)
- fast (ordered) rotation is related to existence of discs,
- slow rotators (ellipticals) actually have large Sérsic indices and often can not be decomposed into two components.

Emsellem+07,11, Krajnovic +11,12
(SAURON, ATLAS3D)

$$\lambda_R \equiv \frac{\langle R\,|V|\rangle}{\langle R\sqrt{V^2+\sigma^2}\rangle}$$

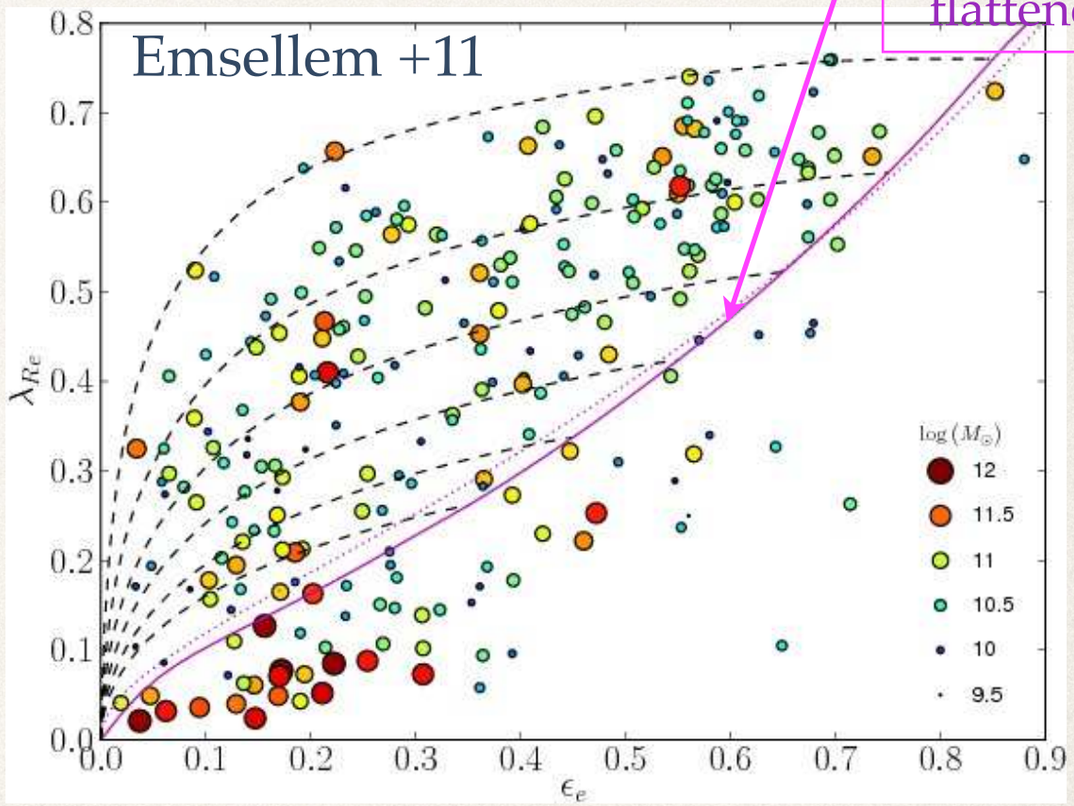

Figure 3. λ_{Re} versus ellipticity ϵ_e for all 260 ATLAS^{3D} galaxies. The colour and size of the symbols are associated with the mass of each galaxy, as indicated at the bottom right of the panel. The dotted magenta line show the edge-on view for ellipsoidal galaxies integrated up to infinity with $\beta = 0.70 \times \epsilon$, as in C+07. The solid magenta line is the corresponding curve restricted to an aperture at 1 R_e and for $\beta = 0.65 \times \epsilon$ (see text for details). The black dashed lines correspond to the location of galaxies with intrinsic ellipticities $\epsilon_{intr} = 0.85, 0.75, 0.65, 0.55, 0.45, 0.35$ along the relation given for an aperture of 1 R_e with the viewing angle going from edge-on (on the relation) to face-on (towards the origin).

The fast-slow rotators dichotomy

- In the traditional classification of early-type galaxies, fast rotators are basically S0s, while slow rotators are true ellipticals

---

- most of early-type galaxies have a significant fraction of stars in discs
- Sérsic indices of bulges of early-type galaxies are often small ($n_b<3$)
- fast (ordered) rotation is related to existence of discs,
- slow rotators (ellipticals) actually have large Sérsic indices and often can not be decomposed into two components.

$$\lambda_R \equiv \frac{\langle R\,|V|\rangle}{\langle R\sqrt{V^2+\sigma^2}\rangle}$$

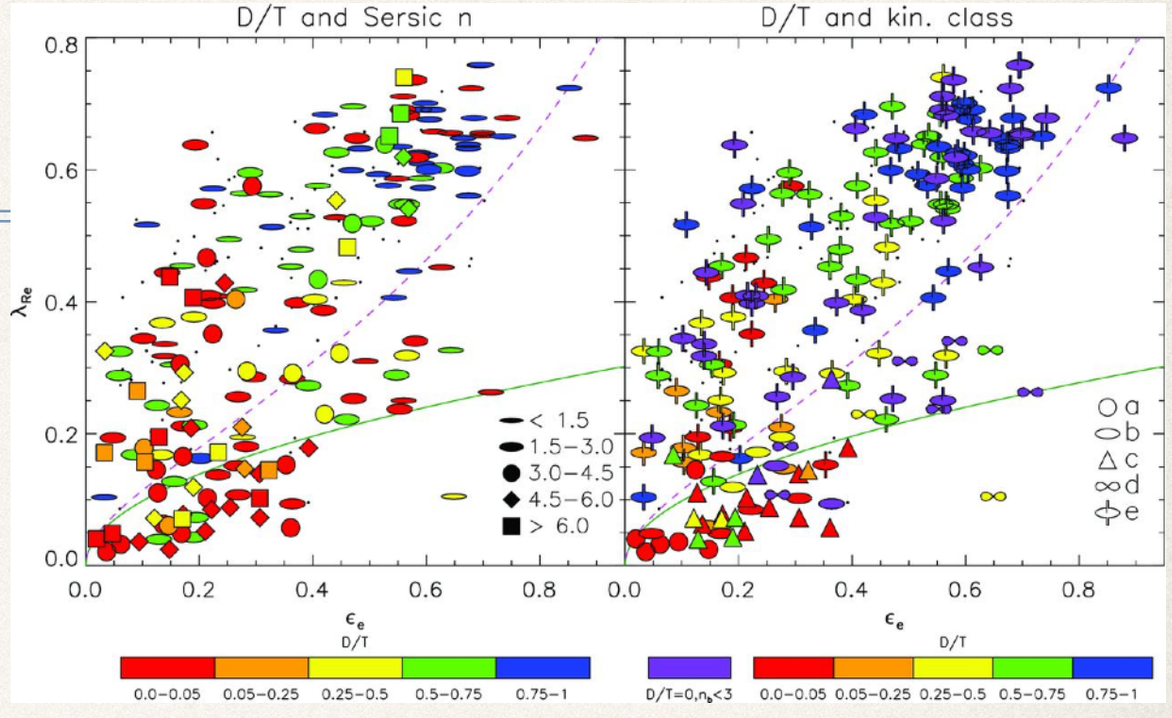

λ*R* versus ϵ for ATLAS**3D** galaxies. Barred galaxies not used for the decomposition are shown as small dots for completeness. Left: symbols represent Sérsic indices as shown in the legend, while colour coding quantifies the *D*/*T* ratio, as shown on the colour bar under the diagram. Right: symbols show different types of kinematics from Paper II and are described in the legend: (a) non-rotating galaxies, (b) featureless non-regular rotators, (c) KDC, (d) 2σ and (e) regular rotators. Colours again quantify *D*/*T* ratios, as shown on the colour bar, but now we also highlight those galaxies which do not have an exponential component, but have *n*b < 3 (purple). The green line separates slow (below the line) from fast (above the line) rotators (Paper III). The dashed magenta line shows the edge-on view for ellipsoidal galaxies with anisotropy β = 0.7ϵ, from Cappellari et al. (2007).

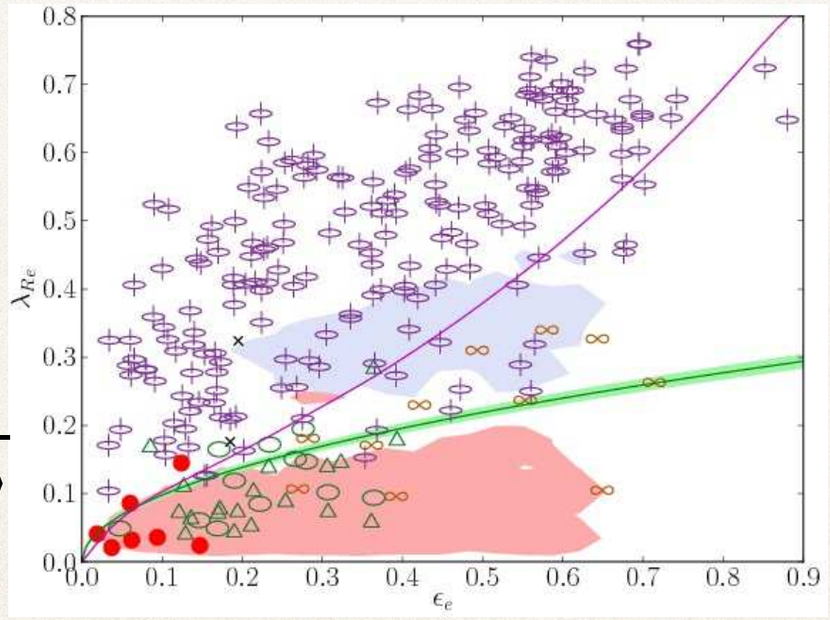

Figure 16. λ_{Re} versus apparent ellipticity ϵ_e within 1 R_e with symbols as in the bottom panel of Fig. 15. The blue and red filled coloured areas show the region where 1:1 and 2:1 merger remnants lie from the study of Bois et al. (2011): the red area corresponds to the merger remnants with a retrograde main progenitor (w.r.t. the orbital angular momentum) while the blue area corresponds to a prograde main progenitor. The green lines show the limit between Slow and Fast Rotators and the magenta line is as in Fig. 7.

Emsellem+11, Krajnovic +12
(SAURON, ATLAS3D)

Kinematically decoupled components

- Indication of some “dramatic event”:

  - accretion of gas with different angular momentum
  - mergers

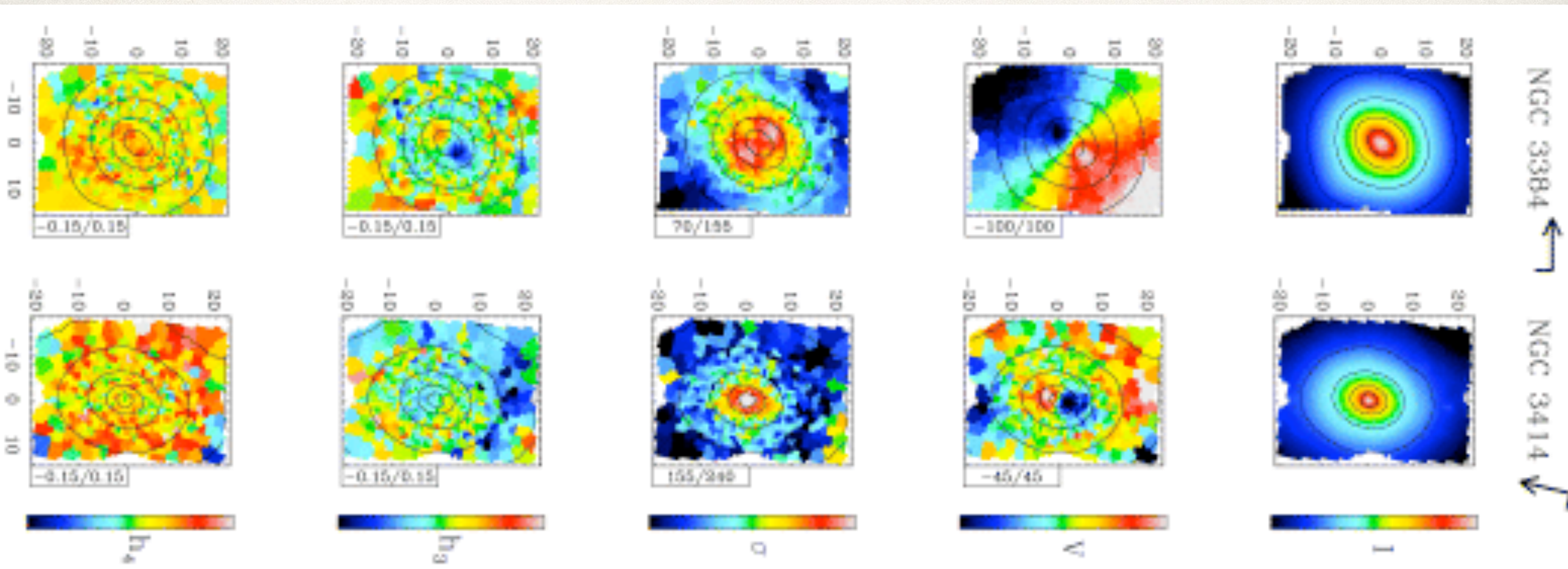

Orbital decompositions for a general galaxy sample

Zhu et al. (Nature Astronomy, 2017 in press, from CALIFA)

$$\lambda_z \equiv J_z / J_{\max}(E)$$

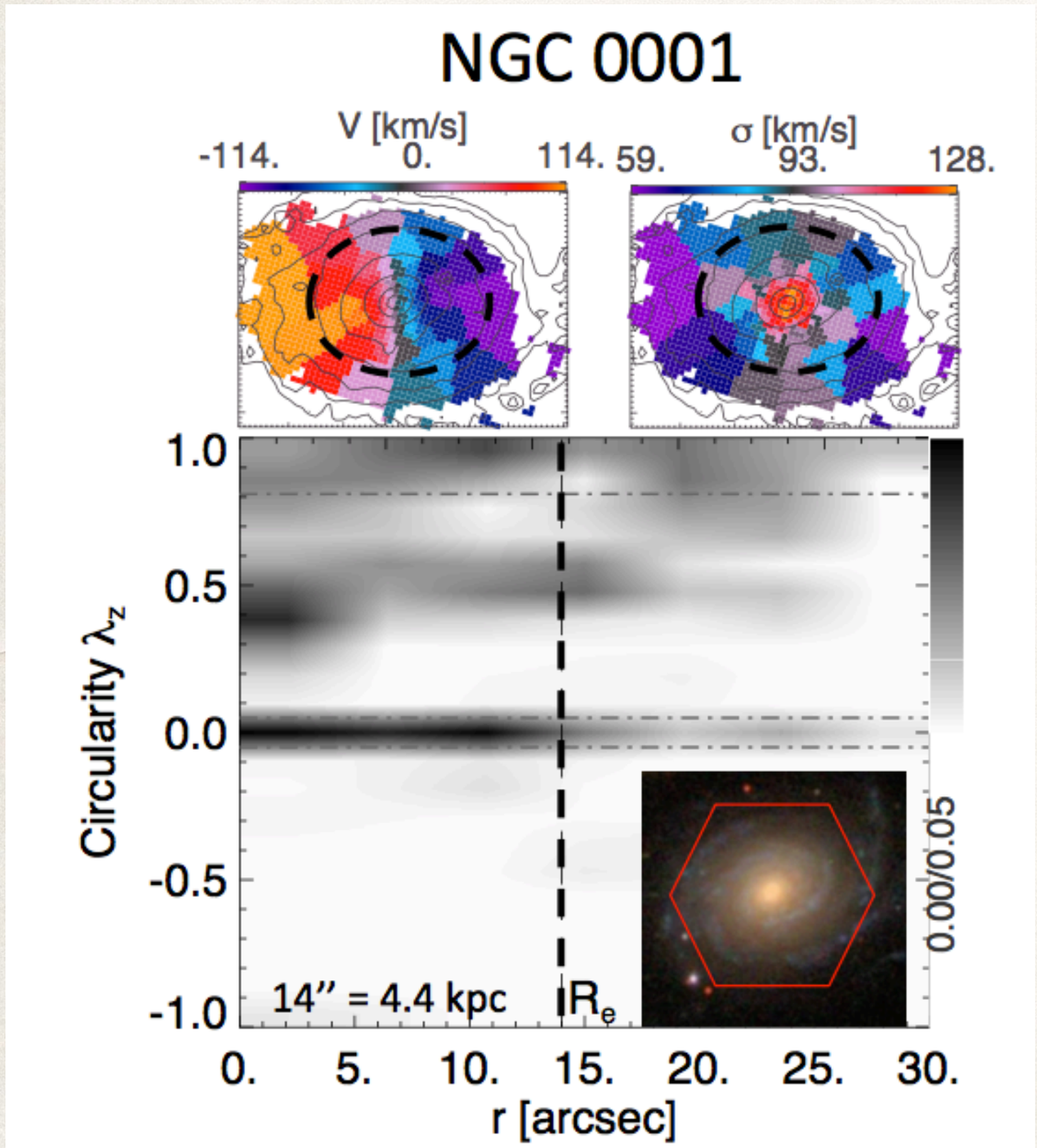

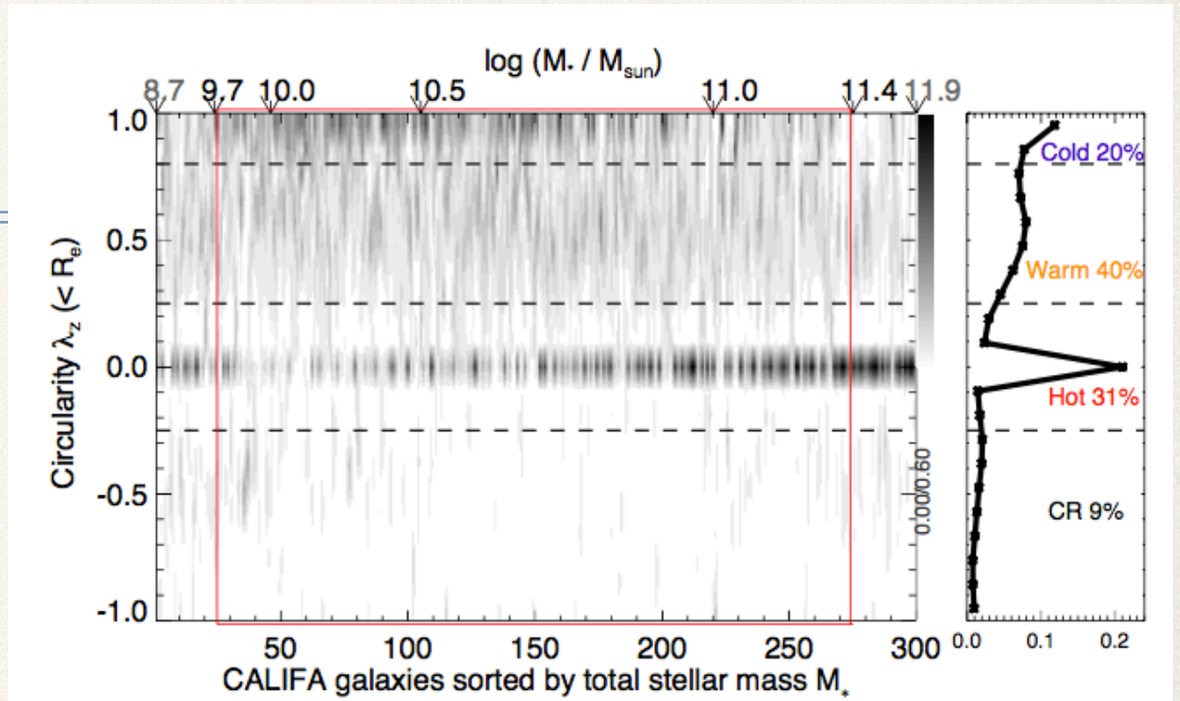

- Cold=circular, disk
- Warm=short-axis tube
- Hot=box and long-axis tube